

Discontinuous functional for linear-response time-dependent density-functional theory: The exact-exchange kernel and approximate forms

Maria Hellgren^{1,2} and E. K. U. Gross²

¹*International School for Advanced Studies (SISSA), via Bonomea 265, 34136 Trieste, Italy*

²*Max-Planck Institute of Microstructure Physics, Weinberg 2, 06120 Halle, Germany*

(Received 3 September 2013; published 13 November 2013)

We present a detailed study of the exact-exchange (EXX) kernel of time-dependent density-functional theory with an emphasis on its discontinuity at integer particle numbers. It was recently found that this exact property leads to sharp peaks and step features in the kernel that diverge in the dissociation limit of diatomic systems [Hellgren and Gross, *Phys. Rev. A* **85**, 022514 (2012)]. To further analyze the discontinuity of the kernel, we here make use of two different approximations to the EXX kernel: the Petersilka Gossmann Gross (PGG) approximation and a common energy denominator approximation (CEDA). It is demonstrated that whereas the PGG approximation neglects the discontinuity, the CEDA includes it explicitly. By studying model molecular systems it is shown that the so-called field-counteracting effect in the density-functional description of molecular chains can be viewed in terms of the discontinuity of the static kernel. The role of the frequency dependence is also investigated, highlighting its importance for long-range charge-transfer excitations as well as inner-shell excitations.

DOI: [10.1103/PhysRevA.88.052507](https://doi.org/10.1103/PhysRevA.88.052507)

PACS number(s): 31.15.ee, 31.15.ag, 31.70.-f

I. INTRODUCTION

Time-dependent density-functional theory (TDDFT) in its linear-response (LR) formulation is a formally exact and computationally efficient method for calculating excited-state properties of many-electron systems [1]. In addition, via the adiabatic connection fluctuation dissipation (ACFD) formula, LR-TDDFT provides a promising approach for determining ground-state properties [2–7].

In TDDFT, the dynamical many-electron density is calculated from a fictitious noninteracting system in which the electrons move in an effective time-dependent Kohn-Sham (KS) potential [8]. The KS potential is the sum of the external, the Hartree, and the unknown exchange-correlation (XC) potential $v_{xc}(\mathbf{r}t)$. The latter is a unique functional of the density and contains all the many-body effects beyond the Hartree level. To linear order in an external perturbing field, only its first variation, evaluated at the ground-state density $n_0(\mathbf{r})$, is required. The central quantity to approximate in LR-TDDFT is thus

$$f_{xc}(\mathbf{r}, \mathbf{r}', t - t') = \left. \frac{\delta v_{xc}(\mathbf{r}t)}{\delta n(\mathbf{r}'t')} \right|_{n=n_0}, \quad (1)$$

known as the XC kernel [9].

Most approximations to f_{xc} are derived from functionals constructed for the ground-state energy. In this way, all history dependence is neglected and f_{xc} becomes independent of frequency. These so-called adiabatic approximations work rather well in many cases. Low-lying molecular excitation energies can be determined quite accurately and even true many-body features such as resonances in the optical spectrum due to the mixing of discrete single-particle states with continuum states are qualitatively described [10–12]. Different studies also show that ground-state properties within the ACFD framework are relatively insensitive to the lack of frequency dependence [3,13]. On the other hand, in the important and challenging cases of charge-transfer, inner-shell, and double excitations, a proper frequency dependence must be included [14–16].

Many works have focused on understanding what features v_{xc} and f_{xc} must have in order to capture different many-body effects. Such an important exact property of v_{xc} , discovered already in the ground-state theory, is the so-called derivative discontinuity [17]. The ground-state XC energy as a function of particle number exhibits kinks at the integers, which reflects the fact that the energy levels of the KS system do not correspond to the true energy levels. In particular, the KS affinity, i.e., the lowest unoccupied KS level, must be corrected with an amount exactly equal to the size of the derivative discontinuity in order to get the true affinity.

A kink in the XC energy leads to a discontinuity in v_{xc} in terms of a constant shift. Although an overall shift can not affect the density, there are fundamental consequences of the discontinuity also for the density. It can appear in subregions of space where the density integrates to a number close to an integer. There, it forms steps which act to prevent delocalization of the charges. This important effect is most clearly demonstrated when breaking chemical bonds [18,19].

For time-dependent problems, very similar steps in the XC potential become important in many situations [20]. For example, it has been shown to be a crucial feature for describing the Coulomb blockade effect in the time domain [21] as well as for accurately reproducing ionization processes [22].

The linear density response function χ is within TDDFT determined from the KS noninteracting response function χ_s according to a Dyson-type equation [23]

$$\chi(\omega) = \chi_s(\omega) + \chi_s(\omega)[v + f_{xc}(\omega)]\chi(\omega), \quad (2)$$

where all quantities are matrices in \mathbf{r}, \mathbf{r}' and v is the bare Coulomb interaction. In insulating solids, a difficulty when calculating the optical spectra from χ is to incorporate the correct band gap since the KS gap, contained in χ_s , in general is much smaller than the true gap [24]. Since the gap is given by the difference between the ionization energy and the affinity, it is expected that the information on how to correct the gap lies in the derivative discontinuity. However, in LR-TDDFT,

that information has to be carried by the XC kernel [25]. A similar situation occurs in the case of charge-transfer (CT) excitations [26]. If one electron is transferred between two fragments, in the limit of infinite separation, the excitation energy is given by the difference in the ionization energy of the donor and the affinity of the acceptor. Again, the latter has to be corrected with the derivative discontinuity. In the case of CT excitations, it has been shown that this correction comes either entirely from the XC kernel or from a combination of the XC potential and the XC kernel [16].

The following question then naturally arises: How does the derivative discontinuity affect the XC kernel? In a recent paper [16], the present authors investigated this question and found a discontinuity of XC kernel with spatial divergencies. Moreover, it was found that the discontinuity could have a strong frequency dependence. The purpose of this paper is to further analyze as well as to present some more examples where the discontinuity of the XC kernel plays an important role.

A framework used for constructing functionals with the derivative discontinuity and with frequency dependence is the variational formulation of many-body perturbation theory (MBPT) [27,28]. An advantage of the MBPT approach to TDDFT is that the relevant physics can be built into the functional via the intuitive Feynman diagram expansions. The first approximation is the so-called time-dependent exact-exchange (TDEXX) approximation, which in MBPT corresponds to the Klein functional at the level of the time-dependent Hartree-Fock (TDHF) approximation. The TDEXX has already been used to calculate many different properties of atoms, molecules, and solids [3,4,12,29–31]. With regards to spectral properties, it has some limitations due to the double inversion of the KS density response function [12], but for ground-state properties within the ACFD framework TDEXX has produced excellent results in terms of total energies, polarizabilities, and van der Waals coefficients [2–4,31]. Furthermore, the static EXX potential exhibits a discontinuity which carries over to the time-dependent potential as shown in Ref. [32].

In this paper, we will study the discontinuity of the TDEXX kernel in order to demonstrate some of its fundamental properties. Apart from studying the exact TDEXX kernel, we also employ two different approximations: a Slater-type of approximation which is also known as the Petersilka Gossmann Gross (PGG) approximation [23] and a Krieger-Li-Iafrate (KLI) type [33] of approximation previously derived in Refs. [34,35]. The latter is here implemented allowing for numerical comparisons. It will be shown that the PGG kernel completely neglects the discontinuity, whereas the KLI approximation incorporates it explicitly.

The paper is organized as follows. We start with a review of the discontinuities in ensemble DFT and then we generalize the discussion to the time-dependent case and derive the discontinuity of the XC kernel. In Sec. III, we present the MBPT framework. In Sec. IV, we derive the Slater and the KLI approximations to the TDEXX kernel. Then, in Sec. V, we present numerical results for different one-dimensional (1D) soft-Coulomb systems. Finally, in Sec. VI, we summarize the main findings.

II. FRACTIONAL CHARGES IN DFT

For functional derivatives to be uniquely defined and for treating densities that integrate to a noninteger number of electrons ensembles must be introduced [17,36]. We will start this section by reviewing ground-state density functionals for ensembles and derive simple formulas for evaluating the discontinuities of a given functional. Then, we will generalize the ensembles to treat systems in time-varying fields and determine the discontinuities of the dynamical XC kernel.

A. Ground-state ensembles

For an average number of electrons $N = N_0 + p$, where N_0 is an integer, it is sufficient to include two members in the ensemble [17]

$$\hat{\gamma}^> = (1 - p)|\Psi_{N_0}\rangle\langle\Psi_{N_0}| + p|\Psi_{N_0+1}\rangle\langle\Psi_{N_0+1}|, \quad (3)$$

where $|\Psi_k\rangle$ is the ground state with k particles. Similarly, for $N = N_0 - 1 + p$ we can define

$$\hat{\gamma}^< = (1 - p)|\Psi_{N_0-1}\rangle\langle\Psi_{N_0-1}| + p|\Psi_{N_0}\rangle\langle\Psi_{N_0}|. \quad (4)$$

The ensemble ground-state energy consists of straight-line segments

$$E^> = (1 - p)E_{N_0} + pE_{N_0+1}, \quad (5)$$

$$E^< = (1 - p)E_{N_0-1} + pE_{N_0} \quad (6)$$

with a derivative discontinuity at the integer N_0 given by $I - A$, where the ionization energy is $I = E_{N_0-1} - E_{N_0}$ and the affinity is $A = E_{N_0} - E_{N_0+1}$.

In this context, the KS system is defined to be the fictitious system of noninteracting electrons that can produce the same ensemble density. The KS ensemble density is given by

$$n^>(\mathbf{r}) = \sum_k^{N_0} |\varphi_k^p(\mathbf{r})|^2 + p|\varphi_{N_0+1}^p(\mathbf{r})|^2, \quad (7)$$

$$n^<(\mathbf{r}) = \sum_k^{N_0-1} |\varphi_k^p(\mathbf{r})|^2 + p|\varphi_{N_0}^p(\mathbf{r})|^2, \quad (8)$$

where the superscript p is attached to denote the fact that the KS potential that determines the orbitals will depend on the average number of particles. The total ground-state ensemble energy can be written as

$$E[n] = T_s[n] + \frac{1}{2} \int d\mathbf{r} d\mathbf{r}' n(\mathbf{r}) v(\mathbf{r}, \mathbf{r}') n(\mathbf{r}') + \int d\mathbf{r} w(\mathbf{r}) n(\mathbf{r}) + E_{xc}[n], \quad (9)$$

where T_s is the noninteracting kinetic energy functional and E_{xc} is the XC energy. In order to exhibit the derivative discontinuity of E_{xc} , we take the derivative with respect to the number of particles

$$\frac{\partial E}{\partial N} = \frac{\partial T_s}{\partial N} + \int d\mathbf{r} [w(\mathbf{r}) + v_H(\mathbf{r})] f(\mathbf{r}) + \frac{\partial E_{xc}}{\partial N}, \quad (10)$$

where we have identified the Fukui function [37]

$$f(\mathbf{r}) = \frac{\partial n(\mathbf{r})}{\partial N}. \quad (11)$$

The derivative of the kinetic energy can easily be evaluated once written in terms of occupied KS eigenvalues ε_k . Let us first focus on an ensemble of the form of Eq. (3), i.e., with $N = N_0 + p$. The derivative with respect to N is equal to the derivative with respect to p and we find

$$\frac{\partial E^>}{\partial N} = \varepsilon_{N_0+1}^> - \int d\mathbf{r} v_{xc}^>(\mathbf{r}) f^>(\mathbf{r}) + \frac{\partial E_{xc}^>}{\partial N} = \varepsilon_{N_0+1}^>, \quad (12)$$

where we have used the identity

$$\frac{\partial E_{xc}}{\partial N} = \int d\mathbf{r} v_{xc}(\mathbf{r}) f(\mathbf{r}) \quad (13)$$

and the definition of the XC potential $v_{xc} = \delta E_{xc}/\delta n$. The same steps can be performed for the ensemble in Eq. (4) and we find similarly

$$\frac{\partial E^<}{\partial N} = \varepsilon_{N_0}^<. \quad (14)$$

Equations (12) and (14) thus prove that the highest occupied eigenvalue must be equal to the chemical potential [36] and should not change with N . Many problems with existing functionals are related to a lack of this straight-line behavior when extended to fractional charges [38–41]. In the limit $N \rightarrow N_0^\pm$ we have

$$\left. \frac{\partial E}{\partial N} \right|_+ = \varepsilon_{N_0+1}^+, \quad \left. \frac{\partial E}{\partial N} \right|_- = \varepsilon_{N_0}^-. \quad (15)$$

In this limit, $\varepsilon_{N_0+1}^+ = \varepsilon_{\text{LUMO}}^+$, i.e., the lowest unoccupied KS orbital obtained from the KS potential in the limit $N \rightarrow N_0^+$ (V_s^+). In the same way, $\varepsilon_{N_0}^- = \varepsilon_{\text{HOMO}}^-$, i.e., the highest occupied KS orbital obtained from V_s^- . It is important from which direction the limit is taken since v_{xc} has a discontinuity at $N = N_0$. The discontinuity in v_{xc} is in general positive, shifting the KS affinity $A_s = -\varepsilon_{\text{LUMO}}^-$ to the true affinity $A = -\varepsilon_{\text{LUMO}}^+$ in order to obey the relation in Eq. (12).

The discontinuity of v_{xc} is related to the derivative discontinuity in $E_{xc}[n[w, N]]$. We can use the identity in Eq. (13) to formally express the value of the discontinuous shift Δ_{xc} at N_0 . For $N > N_0$, we write $v_{xc}^>(\mathbf{r}) = v_{xc}^->(\mathbf{r}) + \Delta_{xc}(\mathbf{r})$ and insert into Eq. (13)

$$\frac{\partial E_{xc}^>}{\partial N} = \int d\mathbf{r} [v_{xc}^->(\mathbf{r}) + \Delta_{xc}(\mathbf{r})] f^>(\mathbf{r}). \quad (16)$$

Taking the limit $N \rightarrow N_0^+$ and by rearranging we find

$$\Delta_{xc} = \left. \frac{\partial E_{xc}}{\partial N} \right|_+ - \int d\mathbf{r} v_{xc}^->(\mathbf{r}) f^+>(\mathbf{r}), \quad (17)$$

where we have used the fact that the Fukui function integrates to unity. If $\partial E_{xc}/\partial N$ has a nontrivial discontinuity at N_0 , Δ_{xc} is finite. A discontinuous shift in the XC potential also implies a shift in the eigenvalues with the same magnitude. Using Eq. (15), we can write

$$-A = \left. \frac{\partial E}{\partial N} \right|_+ = \varepsilon_{\text{LUMO}}^- + \Delta_{xc}. \quad (18)$$

In order to determine the discontinuities of the XC kernel, we start by noting that for particle-number-conserving variations of the density f_{xc} is only defined up to the sum of two arbitrary functions $g_{xc}(\mathbf{r}) + g_{xc}(\mathbf{r}')$. This observation follows

immediately after inspecting the definition of f_{xc} :

$$\delta^2 E_{xc} = \int d\mathbf{r} d\mathbf{r}' \delta n(\mathbf{r}) f_{xc}(\mathbf{r}, \mathbf{r}') \delta n(\mathbf{r}'). \quad (19)$$

When we instead allow for arbitrary density variations, f_{xc} becomes unique but may have a discontinuity of the form

$$f_{xc}^+(\mathbf{r}', \mathbf{r}) - f_{xc}^-(\mathbf{r}', \mathbf{r}) = g_{xc}(\mathbf{r}) + g_{xc}(\mathbf{r}'). \quad (20)$$

In order to evaluate g_{xc} given a functional E_{xc} , we use the same procedure as for the XC potential. Let us study the quantity

$$\begin{aligned} \frac{\delta}{\delta w(\mathbf{r}_1)} \frac{\partial E_{xc}}{\partial N} &= \int d\mathbf{r} d\mathbf{r}' \chi(\mathbf{r}_1, \mathbf{r}) f_{xc}(\mathbf{r}, \mathbf{r}') f(\mathbf{r}') \\ &+ \int d\mathbf{r} v_{xc}(\mathbf{r}) \frac{\delta f(\mathbf{r})}{\delta w(\mathbf{r}_1)}. \end{aligned} \quad (21)$$

Writing $f_{xc}^>(\mathbf{r}', \mathbf{r}) = f_{xc}^->(\mathbf{r}', \mathbf{r}) + g_{xc}(\mathbf{r}, \mathbf{r}')$ and taking the limit $N \rightarrow N_0^+$, $g_{xc}(\mathbf{r}', \mathbf{r}) \rightarrow g_{xc}(\mathbf{r}) + g_{xc}(\mathbf{r}')$ and we arrive at

$$\begin{aligned} &\int d\mathbf{r} \chi(\mathbf{r}_1, \mathbf{r}) g_{xc}(\mathbf{r}) \\ &= \left. \frac{\delta}{\delta w(\mathbf{r}_1)} \frac{\partial E_{xc}}{\partial N} \right|_+ - \int d\mathbf{r} d\mathbf{r}' \chi(\mathbf{r}_1, \mathbf{r}) f_{xc}^->(\mathbf{r}, \mathbf{r}') f^+>(\mathbf{r}') \\ &- \int d\mathbf{r} v_{xc}^+>(\mathbf{r}) \frac{\delta f^+>(\mathbf{r})}{\delta w(\mathbf{r}_1)}. \end{aligned} \quad (22)$$

This equation only determines g_{xc} up to constant. The constant can, however, be fixed by considering the second derivative of E_{xc} with respect to N :

$$\begin{aligned} 2 \int d\mathbf{r} f^+>(\mathbf{r}) g_{xc}(\mathbf{r}) &= \left. \frac{\partial^2 E_{xc}}{\partial N^2} \right|_+ - \int d\mathbf{r}' v_{xc}^+>(\mathbf{r}') \frac{\partial f^+>(\mathbf{r}')}{\partial N} \\ &- \int d\mathbf{r} d\mathbf{r}' f^+>(\mathbf{r}) f_{xc}^->(\mathbf{r}, \mathbf{r}') f^+>(\mathbf{r}'), \end{aligned} \quad (23)$$

yielding a condition to be imposed on Eq. (22). The function g_{xc} obtained via Eqs. (22) and (23) was recently analyzed in Ref. [16] showing a diverging behavior of the form

$$g_{xc}(\mathbf{r}) \sim \frac{|\varphi_{N_0+1}(\mathbf{r})|^2}{n(\mathbf{r})} \sim e^{2(\sqrt{2I} - \sqrt{2A_s})r}, \quad (24)$$

as $r \rightarrow \infty$. In the next section, we will generalize these ideas to TDDFT.

B. Time-dependent ensembles

The discontinuity, found as an exact property in the ground-state XC potential, appears also in the time-dependent XC potential. In, e.g., an ionization process, the particle number will change locally on the molecule and hence v_{xc} around the molecule will be evaluated close to an integer [22]. In the case of quantum transport, electrons are transferred from a lead to a weakly connected central region, which could be a quantum dot or a molecule. In order to describe the Coulomb blockade effect, it has been shown that in the central region v_{xc} forms a step, which has been associated with the derivative discontinuity [21].

In the time-dependent case, the discontinuity will be rather different from the ground-state discontinuity. The size of the jump will depend on the density at the time when the

particle number crosses an integer. That density may not be the ground-state density. Also, a history dependence could be important [20]. As a consequence, in TDDFT the analysis of the discontinuities of a given functional becomes much more complicated. In this work we will, however, not aim for such a general description of the discontinuity of the time-dependent XC potential. Instead, we will focus only on the linear-response regime, in which the kernel depends only on time differences. Numerical results suggest that the discontinuity of the XC kernel also carries a frequency dependence [16,20]. To see that a frequency dependence in principle is allowed for, we examine the definition of the dynamical kernel for particle-number-conserving density variations $\delta n(\mathbf{r}, \omega)$:

$$\delta v_{xc}(\mathbf{r}, \omega) = \int d\mathbf{r}' f_{xc}(\mathbf{r}, \mathbf{r}', \omega) \delta n(\mathbf{r}', \omega). \quad (25)$$

From this definition, we see that we can always add two functions $g_{xc}(\mathbf{r}, \omega)$ and $g_{xc}(\mathbf{r}', \omega)$ to f_{xc} without changing the physical results obtained from the density response function. The function $g_{xc}(\mathbf{r}, \omega)$ will clearly vanish when integrating over \mathbf{r}' and the function $g_{xc}(\mathbf{r}', \omega)$ will merely generate an irrelevant constant to v_{xc} . In order to make the functional derivative unique, we thus need to allow for variations that can change the particle numbers.

Given a general functional $F[n]$, its functional derivative with respect to $n(\mathbf{r}t)$ is defined as

$$\delta F[n] = \int d\mathbf{r} dt \frac{\delta F}{\delta n(\mathbf{r}t)} \delta n(\mathbf{r}t), \quad (26)$$

where the integral over time is taken over the interval $[0, T]$. If the density variations conserve the particle numbers, $\delta F/\delta n(\mathbf{r}t)$ is only defined up to a function $C(t)$. Allowing a change of particle numbers that is constant in time removes some of the arbitrariness but leaves the derivative still undefined up to a function $S(t)$ with the property

$$\int dt S(t) = 0. \quad (27)$$

We thus see that we have to allow the particle number to change in time in order to completely fix the functional derivatives, which suggests that we need ensembles that vary the particle number in time in order to exhibit the discontinuities of a given functional. To see this more clearly, we start by defining ensembles as in Eqs. (3) and (4) but now replacing the ground states of the N and $N + 1$ particle systems with states that evolve in time in the external potential $w(t)$. Let us now consider the N derivative of the XC potential, defined on the ensemble densities, and evaluate it at the ground-state density with $N = N_0^+$, i.e., $n(\mathbf{r}t) = n_0^+(\mathbf{r})$:

$$\begin{aligned} \left. \frac{\delta v_{xc}(\mathbf{r}t)}{\delta N} \right|_{n_0^+} &= \int d\mathbf{r}' dt' f_{xc}^-(\mathbf{r}, \mathbf{r}', t - t') f^+(\mathbf{r}') \\ &+ \int d\mathbf{r}' dt' g_{xc}(\mathbf{r}', t - t') f^+(\mathbf{r}') \\ &+ \int dt' g_{xc}(\mathbf{r}, t - t'). \end{aligned} \quad (28)$$

Clearly, this equation does not allow us to completely determine the discontinuity g_{xc} . We therefore propose an ensemble where also the coefficients vary in time and thus allows the

particle number to change as a function of time. We write

$$\begin{aligned} \hat{\gamma}^>(t) &= \{1 - p_1(t)\} |\Psi_{N_0}(t)\rangle \langle \Psi_{N_0}(t)| \\ &+ p_1(t) |\Psi_{N_0+1}(t)\rangle \langle \Psi_{N_0+1}(t)|, \end{aligned} \quad (29)$$

$$\begin{aligned} \hat{\gamma}^<(t) &= \{1 - p_2(t)\} |\Psi_{N_0-1}(t)\rangle \langle \Psi_{N_0-1}(t)| \\ &+ p_2(t) |\Psi_{N_0}(t)\rangle \langle \Psi_{N_0}(t)|, \end{aligned} \quad (30)$$

where $p_1(t)$ and $p_2(t)$ are two arbitrary functions that can vary between 0 and 1. The time-dependent numbers of particles are then $N^>(t) = N_0 + p_1(t)$ and $N^<(t) = N_0 - 1 + p_2(t)$, respectively. We are only interested in the linear response which means that the functionals should be evaluated at the ground-state density. Assuming that $p_1(t_0) = 0^+$, i.e., $N(t_0) = N_0^+$, where t_0 is the initial time, we compare this kernel $f_{xc}^+(\mathbf{r}, \mathbf{r}', \omega)$ to the one evaluated at $p_2(t_0) = 1^-$, i.e., $N(t_0) = N_0^-$ denoted $f_{xc}^-(\mathbf{r}, \mathbf{r}', \omega)$. These kernels are thus evaluated at the same ground-state density, the only difference being from which side of the integer the limit is taken. Now let us use Eq. (29), take the derivative of v_{xc} with respect to the time-dependent number of particles, and evaluate it at $n_0^+ = n^+(\mathbf{r}t_0)$:

$$\begin{aligned} \left. \frac{\delta v_{xc}(\mathbf{r}t)}{\delta N(t')} \right|_{n_0^+} &= \int d\mathbf{r}' f_{xc}^-(\mathbf{r}, \mathbf{r}', t - t') f^+(\mathbf{r}') \\ &+ \int d\mathbf{r}' g_{xc}(\mathbf{r}', t - t') f^+(\mathbf{r}') + g_{xc}(\mathbf{r}, t - t'). \end{aligned} \quad (31)$$

The function $g_{xc}(\mathbf{r}, \omega)$ can now be determined. The ensemble proposed thus allows functional derivatives to be uniquely defined.

In the next section, we will study $g_{xc}(\mathbf{r}, \omega)$ within the TDEXX approximation.

III. RESTRICTED KLEIN FUNCTIONAL

In this section, we will introduce a framework for constructing advanced functionals for DFT and TDDFT [27]. The basic idea is to use the Klein action functional [42] formulated in terms of the many-body Green's function G , and then to restrict the variational freedom to KS Green's functions G_s coming from a local multiplicative KS potential V .

The Klein functional is defined as

$$iY_K[G] = \Phi[G] - \text{Tr} \{ G G_0^{-1} - 1 + \ln(-G^{-1}) \}, \quad (32)$$

where G_0 is the noninteracting ‘‘bare’’ Green's function carrying information about the external potential w and the number of particles. The trace Tr denotes a sum over one electron state plus an integral over the Keldysh contour [43]. The functional Φ is constructed such that the self-energy Σ is given by

$$\Sigma = \frac{\delta \Phi}{\delta G}. \quad (33)$$

Varying the Klein functional with respect to G yields the Dyson equation

$$G = G_0 + G_0 \Sigma G, \quad (34)$$

as a condition that renders the functional stationary. Furthermore, for static problems the stationary point of the Klein functional is equal to the total energy $iY_K = E^{\text{tot}}$. Not all possible

approximate self-energies can be constructed from a Φ functional as can easily be verified to third order in the Coulomb interaction. The set of those self-energies that can be called Φ -derivable or *conserving* approximations since it can be shown that the resulting G incorporates basic conservation laws such as energy, particle, and momentum conservation [44].

By restricting the variational freedom to KS Green's functions, we simply replace G by G_s in Eq. (32). The noninteracting G_s is easily constructed, and in the static case the Klein functional simplifies to

$$Y_K[V] = T_s[n] + \int d\mathbf{r} w(\mathbf{r})n(\mathbf{r}) - i\Phi[G_s], \quad (35)$$

where T_s is the kinetic energy of noninteracting electrons in the potential V . The Φ functional thus plays the role of the Hartree and XC energy [27,28]. In this way, we can generate approximate functionals in DFT and TDDFT from Φ -derivable self-energies in MBPT. These functionals are implicit, nonlocal density functionals via G_s , which depend on KS orbitals and eigenvalues. Therefore, they can overcome some of the limitations involved in local and explicit functionals of the density. Moreover, the hope is that the physics included in the self-energy is reflected in the performance of the density functional as well. The level to which this is true has recently been investigated [45].

We can now use standard TDDFT results to determine the XC potential v_{xc} . Using the chain rule $\delta\Phi^{xc}/\delta G_s * \delta G_s/\delta V = \delta\Phi^{xc}/\delta n * \delta n/\delta V$ we find the so-called linearized Sham-Schlüter (LSS) equation [46] (with $\mathbf{r}_1 t_1 \rightarrow 1$)

$$\int \chi_s(1,2)v_{xc}(2)d2 = \int \Sigma_s^{xc}(2,3)\Lambda(3,2;1)d2 d3, \quad (36)$$

where Σ_s^{xc} is the self-energy calculated with KS orbitals generated by V and

$$i\Lambda(3,2;1) = \frac{\delta G_s(3,2)}{\delta V(1)} = G_s(3,1)G_s(1,2).$$

A further variation of the LSS equation with respect to the potential V results in an equation for f_{xc} :

$$\begin{aligned} & \int \chi_s(1,2)f_{xc}(2,3)\chi_s(3,4)d2 d3 \\ &= \int \frac{\delta \Sigma_s^{xc}(2,3)}{\delta V(4)}\Lambda(3,2;1)d2 d3 \\ &+ \int \Lambda(1,2;4)D(2,3)G_s(3,1)d2 d3 \\ &+ \int G_s(1,2)D(2,3)\Lambda(3,1;4)d2 d3, \end{aligned} \quad (37)$$

where $D(2,3) = \Sigma_s^{xc}(2,3) - v_{xc}(2)\delta(2,3)$.

The XC functional derived from the Klein functional approach has been shown to generate XC potentials which have many features of the exact XC potential. Of particular interest for this work is the derivative discontinuity, which is well reproduced at least at even integer electron number.

In order to investigate these functionals for densities that integrate to a noninteger particle number, we will here assume that the proper generalization is made by inserting an ensemble KS Green's function G_s^E constructed from the ensembles introduced in Sec. II (see Ref. [16]). This has proven to be the right procedure using Hartree-Fock (HF) and GW self-energies [47]. Using Eq. (17), we can express the discontinuity of the ensemble v_{xc}^E as [16,17]

$$\begin{aligned} \Delta_{xc} &= \int d\mathbf{r} d\mathbf{r}' \varphi_L(\mathbf{r})[\Sigma_s^{xc}[G_s^+](\mathbf{r},\mathbf{r}',\varepsilon_L^+) \\ &- v_{xc}^-(\mathbf{r}')\delta(\mathbf{r} - \mathbf{r}')] \varphi_L(\mathbf{r}'), \end{aligned} \quad (38)$$

where φ_L is the LUMO orbital of the N^- system and $\varepsilon_L^+ = \varepsilon_L^- + \Delta_{xc}$. At any given N , the ensemble v_{xc}^E is determined by Eq. (36) by replacing $\Sigma_s^{xc}[G_s]$ with $\Sigma_s^{xc}[G_s^E]$, Λ with Λ^E , and χ_s with χ_s^E . v_{xc}^E is, however, not uniquely determined by Eq. (36), but only up to a constant. This constant can be fixed using Eq. (13). For instance, when $N < N_0$, we find

$$0 = \langle \varphi_H | \Sigma_s^{xc}[G_s^E](\varepsilon_H) - v_{xc}^E | \varphi_H \rangle \quad (39)$$

(in bracket notation). This condition results in $v_{xc}^E(\mathbf{r}) \rightarrow 0$ when $\mathbf{r} \rightarrow \infty$.

Similarly, the *static* ensemble XC kernel can be evaluated from the second derivative of Eq. (36), leading to an equation similar to Eq. (37) at $\omega = 0$. The nonuniqueness now amounts to a function depending on \mathbf{r} in both inversions of χ_s^E . In order to fix these functions, we proceed as follows. For the first inversion, Eq. (21) can be used directly as a condition to impose on Eq. (37). In the second inversion, we need a condition of the kind $\int d\mathbf{r} f_{xc}(\mathbf{r}',\mathbf{r})q(\mathbf{r}) = Q(\mathbf{r}')$. Such condition can be found from Eq. (21) by imposing Eq. (23) and solve for $\int d\mathbf{r} f_{xc}(\mathbf{r}',\mathbf{r})f(\mathbf{r})$.

In order to write an equation for the discontinuity of f_{xc}^E at any given frequency, the time-dependent ensembles (29) and (30) must be used. The derivative in Eq. (31) can be evaluated by taking the derivative of Eq. (36), assuming χ_s , G_s , Λ , and n are obtained as expectation values of Eqs. (29) and (30). That this generalization makes sense is not obvious and each approximation should be carefully investigated independently. However, if we apply this assumption, we find the following equation determining the frequency-dependent discontinuity:

$$\begin{aligned} \int d\mathbf{r}_2 \chi_s(\mathbf{r}_1, \mathbf{r}_2, \omega) g_{xc}(\mathbf{r}_2, \omega) &= \int d2 d3 \Sigma_s^{xc}(2,3) \frac{\delta \Lambda(2,3;1)}{\delta N(t)} \Big|_{n_0^+} + \int d(2345) \frac{\delta \Sigma_s^{xc}(2,3)}{\delta G_s(4,5)} \frac{\delta G_s(4,5)}{\delta N(t)} \Lambda(3,2;1) \Big|_{n_0^+} \\ &- \int d\mathbf{r}_2 d\mathbf{r}_3 \chi_s(\mathbf{r}_1, \mathbf{r}_2, \omega) f_{xc}^-(\mathbf{r}_2, \mathbf{r}_3, \omega) f^+(\mathbf{r}_3) - \int d2 v_{xc}^+(2) \frac{\delta \chi_s(1,2)}{\delta N(t)} \Big|_{n_0^+}. \end{aligned} \quad (40)$$

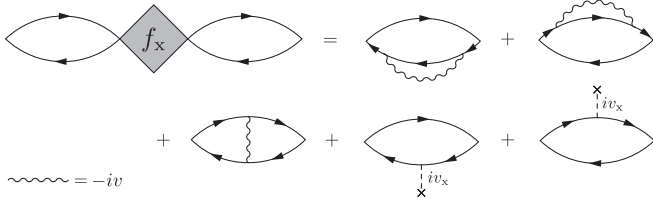


FIG. 1. Diagrammatic representation of Eq. (37) in the EXX approximation. Solid arrowed lines represent time-ordered Green's functions.

In the limit $\omega = 0$, this equation reduces to the equation obtained by considering a static ensemble. We note also that, in linear response, all quantities are evaluated at the ground state and hence the precise form of $N(t)$ in time will not enter the equation. Equation (40) determines g_{xc} up to a constant. At $\omega = 0$, we can use Eq. (23) to fix this constant. For $\omega \neq 0$, it is not clear how to fix the constant since we started from an equation that can not completely determine the ensemble v_{xc} .

Until now, functionals based on the Klein expression have been studied in the HF approximation, the second-order Born, and the GW, corresponding to the EXX, MP2, and RPA, respectively, in the restricted density-functional framework. In the time-dependent linear-response regime, only the TDEXX kernel has been implemented for atoms. The frequency dependence found had some deficiencies, indicating that exchange effects might have to be treated more carefully when translated from MBPT to TDDFT. In the next section, we will mainly focus on the static kernel and investigate its discontinuities in detail. This will be done with the help of

$$\int d\mathbf{r}_2 \chi_s(\mathbf{r}_1, \mathbf{r}_2, \omega) g_{xc}(\mathbf{r}_2, \omega) = 4 \sum_{k \neq L} \int d\mathbf{r}_2 d\mathbf{r}_3 [v(\mathbf{r}_2, \mathbf{r}_3) \gamma(\mathbf{r}_2, \mathbf{r}_3) - v_x^+(\mathbf{r}_2) \delta(\mathbf{r}_2, \mathbf{r}_3)] \frac{\varphi_L(\mathbf{r}_2) \varphi_k(\mathbf{r}_3) \varphi_L(\mathbf{r}_1) \varphi_k(\mathbf{r}_1) \varepsilon_{kL}}{\omega^2 - \varepsilon_{kL}^2} + \frac{1}{2} \int d\mathbf{r}_2 d\mathbf{r}_3 v(\mathbf{r}_3, \mathbf{r}_2) \varphi_L(\mathbf{r}_2) \varphi_L(\mathbf{r}_3) \Lambda(\mathbf{r}_3, \mathbf{r}_2; \mathbf{r}_1, \omega) - \int d\mathbf{r}_2 d\mathbf{r}_3 \chi_s(\mathbf{r}_1, \mathbf{r}_2, \omega) f_{xc}^-(\mathbf{r}_2, \mathbf{r}_3, \omega) |\varphi_L(\mathbf{r}_3)|^2. \quad (44)$$

We note that this equation is the limit $N \rightarrow N_0^+$ of the equation used for uniquely determining f_x .

A very useful and accurate approximation to the EXX potential is the so-called KLI approximation [33]. Apart from leading to a potential and kernel which may have numerical advantages, the KLI approximation exhibits the discontinuity in an instructive way. The KLI approximation avoids the inversion of the full χ_s by means of a common energy denominator approximation (CEDA). The CEDA sets all KS excitation energies to the same value $\Delta\varepsilon$. In the retarded χ_s , this procedure amounts to the following:

$$\chi_s(\mathbf{r}_1, \mathbf{r}_2; \omega) = 4 \sum_{kk'} n_k (1 - n_{k'}) \frac{\varepsilon_{k'} - \varepsilon_k}{\omega^2 - (\varepsilon_{k'} - \varepsilon_k)^2} \times \varphi_k(\mathbf{r}_1) \varphi_{k'}(\mathbf{r}_1) \varphi_k(\mathbf{r}_2) \varphi_{k'}(\mathbf{r}_2)$$

common energy denominator approximations. We will also investigate the role of the frequency dependence.

IV. EXACT EXCHANGE AND THE KLI APPROXIMATION

In this section, we will focus on the TDEXX approximation which corresponds to the TDHF approximation within MBPT. In the TDEXX we have

$$\Phi^x = \frac{i}{2} \text{Tr} [G_s G_s v], \quad \Sigma_s^x(1,2) = i G_s(1,2) v(1,2). \quad (41)$$

For calculating the TDEXX kernel from Eq. (37), we also need the variation of the self-energy with respect to V :

$$\frac{\delta \Sigma_s^x(2,3)}{\delta V(4)} = -v(2,3) \Lambda(2,3;4).$$

The terms on the right-hand side of Eq. (37) can be represented diagrammatically as in Fig. 1. Evaluating the trace in Eq. (41), we find the standard expression for the ground-state EXX energy

$$E_x = -i \Phi_s^x = - \int d\mathbf{r} d\mathbf{r}' \gamma(\mathbf{r}, \mathbf{r}') v(\mathbf{r}, \mathbf{r}') \gamma(\mathbf{r}, \mathbf{r}'), \quad (42)$$

in terms of the KS density matrix $\gamma(\mathbf{r}, \mathbf{r}') = \sum_k n_k \varphi_k(\mathbf{r}) \varphi_k(\mathbf{r}')$, where n_k is the occupation number of orbital k which can be either zero (unoccupied) or one (occupied). The discontinuity of the static EXX potential is equal to

$$\Delta_x = \int d\mathbf{r} d\mathbf{r}' \varphi_L(\mathbf{r}) [\Sigma_x(\mathbf{r}, \mathbf{r}') - v_x^-(\mathbf{r}') \delta(\mathbf{r}, \mathbf{r}')] \varphi_L(\mathbf{r}'), \quad (43)$$

where $\Sigma_x(\mathbf{r}, \mathbf{r}') = -\gamma(\mathbf{r}, \mathbf{r}') v(\mathbf{r}, \mathbf{r}')$. The discontinuity of the TDEXX kernel can be determined using Eq. (40). We find

$$\begin{aligned} &\approx A(\omega) \sum_{kk'} n_k (1 - n_{k'}) \varphi_k(\mathbf{r}_1) \varphi_{k'}(\mathbf{r}_1) \varphi_k(\mathbf{r}_2) \varphi_{k'}(\mathbf{r}_2) \\ &= A(\omega) \gamma(\mathbf{r}_1, \mathbf{r}_2) [\delta(\mathbf{r}_1, \mathbf{r}_2) - \gamma(\mathbf{r}_1, \mathbf{r}_2)], \end{aligned} \quad (45)$$

where $A(\omega) = 4\Delta\varepsilon/(\omega^2 - \Delta\varepsilon^2)$. We will now use Eq. (45), perform a similar approximation to Λ_s , and simplify Eq. (36). In this way, as a first step, we obtain the so-called localized HF approximation (LHF) [34,48]

$$\begin{aligned} v_x^{\text{LHF}}(\mathbf{r}_1) &= \frac{\int d\mathbf{r}_2 \Sigma_x(\mathbf{r}_1, \mathbf{r}_2) \gamma(\mathbf{r}_2, \mathbf{r}_1)}{\gamma(\mathbf{r}_1)} \\ &+ \sum_{kk'} n_k n_{k'} \frac{\varphi_k(\mathbf{r}_1) \varphi_{k'}(\mathbf{r}_1)}{\gamma(\mathbf{r}_1)} \langle \varphi_k | D_x | \varphi_{k'} \rangle, \end{aligned} \quad (46)$$

where we have defined $D_x(\mathbf{r}, \mathbf{r}') = v_x(\mathbf{r}) \delta(\mathbf{r}, \mathbf{r}') - \Sigma_x(\mathbf{r}, \mathbf{r}')$ and $\gamma(\mathbf{r}) = \gamma(\mathbf{r}, \mathbf{r})$. The first term can be identified as the Slater

potential $v_x^S(\mathbf{r}_1)$ [49]. Making the further approximation of retaining only the diagonal elements of the second term, we find the aforementioned KLI approximation [33]

$$v_x^{\text{KLI}}(\mathbf{r}_1) = v_x^S(\mathbf{r}_1) + \sum_k n_k \frac{|\varphi_k(\mathbf{r}_1)|^2}{\gamma(\mathbf{r}_1)} \langle \varphi_k | D_x | \varphi_k \rangle. \quad (47)$$

The KLI potential v_x^{KLI} has shown to be a very good approximation to the true EXX potential. Performing a similar approximation to self-energies which contain correlation is less straightforward due to the extra energy dependence of a self-energy with correlation. However, using some additional approximation, such equations have been derived by Casida [28].

The KLI potential is undetermined up to the addition of a constant. However, applying Eq. (39) ensures that also $v_x^{\text{KLI}} \rightarrow 0$ as $r \rightarrow \infty$ [33]. We notice the similarity of the second term

to the expression for the discontinuity within EXX [Eq. (43)]. Indeed, it is easy to see that this is exactly the term that gives rise to steps in v_x^{KLI} [19]. These steps are of the same origin as the derivative discontinuity. The Slater potential misses any such features.

We will now study the TDEXX kernel in similar approximations (from now on called the EXX kernel). The Slater or the KLI approximations to the EXX kernel could be defined as the functional derivatives of the corresponding potentials. This would, however, lead to equations where the full χ_s has to be inverted. Instead, we start directly from the equation for the kernel. The left-hand side of Eq. (37) contains two χ_s which both are replaced with Eq. (45). The right-hand side contains only energy differences between unoccupied and occupied KS states, thus permitting a similar CEDA. We find on the left-hand side

$$\begin{aligned} & \int d\mathbf{r}_2 d\mathbf{r}_3 \chi_s(\mathbf{r}_1, \mathbf{r}_2; \omega) f_x(\mathbf{r}_2, \mathbf{r}_3; \omega) \chi_s(\mathbf{r}_3, \mathbf{r}_4; \omega) \\ & \approx A^2(\omega) \gamma(\mathbf{r}_1) f_x^{\text{LHF}}(\mathbf{r}_1, \mathbf{r}_4; \omega) \gamma(\mathbf{r}_4) - A^2(\omega) \gamma(\mathbf{r}_1) \int d\mathbf{r}_3 f_x^{\text{LHF}}(\mathbf{r}_1, \mathbf{r}_3; \omega) \gamma^2(\mathbf{r}_3, \mathbf{r}_4) \\ & \quad - A^2(\omega) \gamma(\mathbf{r}_4) \int d\mathbf{r}_2 \gamma^2(\mathbf{r}_1, \mathbf{r}_2) f_x^{\text{LHF}}(\mathbf{r}_2, \mathbf{r}_4; \omega) + A^2(\omega) \int d\mathbf{r}_2 d\mathbf{r}_3 \gamma^2(\mathbf{r}_1, \mathbf{r}_2) f_x^{\text{LHF}}(\mathbf{r}_2, \mathbf{r}_3; \omega) \gamma^2(\mathbf{r}_3, \mathbf{r}_4). \end{aligned} \quad (48)$$

Details on the simplifications of the right-hand side can be found in the Appendix. Here, we simply state the result

$$\begin{aligned} R(\mathbf{r}_1, \mathbf{r}_4; \omega) = & -\frac{A^2(\omega)}{2} \left[\gamma^2(\mathbf{r}_4, \mathbf{r}_1) v(\mathbf{r}_1, \mathbf{r}_4) + \int d\mathbf{r}_2 \Sigma_s^x(\mathbf{r}_1, \mathbf{r}_2) \Gamma(\mathbf{r}_2, \mathbf{r}_1; \mathbf{r}_4) + \int d\mathbf{r}_2 \Sigma_s^x(\mathbf{r}_4, \mathbf{r}_2) \Gamma(\mathbf{r}_2, \mathbf{r}_4; \mathbf{r}_1) \right. \\ & \left. + \int d\mathbf{r}_2 d\mathbf{r}_3 \Gamma(\mathbf{r}_3, \mathbf{r}_2; \mathbf{r}_4) v(\mathbf{r}_3, \mathbf{r}_2) \Gamma(\mathbf{r}_3, \mathbf{r}_2; \mathbf{r}_1) - \alpha_\varepsilon(\omega) \{ B(\mathbf{r}_1, \mathbf{r}_4) \gamma(\mathbf{r}_4, \mathbf{r}_1) + B(\mathbf{r}_4, \mathbf{r}_1) \gamma(\mathbf{r}_4, \mathbf{r}_1) \} \right], \end{aligned} \quad (49)$$

where

$$B(\mathbf{r}_1, \mathbf{r}_4) = \int d\mathbf{r}_2 D_x(\mathbf{r}_1, \mathbf{r}_2) \gamma(\mathbf{r}_2, \mathbf{r}_4) - \int d\mathbf{r}_2 d\mathbf{r}_3 \gamma(\mathbf{r}_1, \mathbf{r}_2) D_x(\mathbf{r}_2, \mathbf{r}_3) \gamma(\mathbf{r}_3, \mathbf{r}_4) \quad (50)$$

and $\Gamma(\mathbf{r}_3, \mathbf{r}_2; \mathbf{r}_1) = \gamma(\mathbf{r}_2, \mathbf{r}_1) \gamma(\mathbf{r}_1, \mathbf{r}_3)$ and $\alpha_\varepsilon(\omega) = (3\varepsilon^2 - \omega^2)/2\varepsilon^2$. In the static limit ($\omega = 0$), the same result for f_x^{LHF} was found in Refs. [34,35]. We notice that only the density matrix with occupied orbitals appears. In Fig. 2, Eqs. (48) and (49) is represented graphically which reveals better the structure of the equation. We see that the original equation is transformed from an equation where the Green's function is the basic variable to an equation where the density matrix is the basic variable. After division with the density we identify the first term to be the PGG kernel [23]

$$f_x^{\text{PGG}}(\mathbf{r}_1, \mathbf{r}_4) = -\frac{1}{2} \frac{\gamma^2(\mathbf{r}_4, \mathbf{r}_1) v(\mathbf{r}_1, \mathbf{r}_4)}{\gamma(\mathbf{r}_1) \gamma(\mathbf{r}_4)}. \quad (51)$$

In analogy with the Slater potential, the PGG kernel is obtained by ignoring the second term in the approximate response function of Eq. (45). This term gives rise to the ‘‘response’’ part of the LHF kernel as discussed in Ref. [34]. With the aim of studying the discontinuity of the kernel, it is essential to keep also this term as we will now see. We will make the further approximation of KLI, which means that we retain only diagonal terms in k, k' . Hence,

$$f_x^{\text{KLI}}(\mathbf{r}_1, \mathbf{r}_4; \omega) = f_x^{\text{PGG}}(\mathbf{r}_1, \mathbf{r}_4) + f_x^{\text{DD}}(\mathbf{r}_1, \mathbf{r}_4; \omega), \quad (52)$$

where

$$\begin{aligned} f_x^{\text{DD}}(\mathbf{r}_1, \mathbf{r}_4; \omega) = & -\sum_k^{\text{occ}} \frac{|\varphi_k(\mathbf{r}_4)|^2}{\gamma(\mathbf{r}_4)} \left[\frac{1}{2} \frac{\varphi_k(\mathbf{r}_1)}{\gamma(\mathbf{r}_1)} \int d\mathbf{r}_2 \Sigma_x(\mathbf{r}_1, \mathbf{r}_2) \varphi_k(\mathbf{r}_2) - \int d\mathbf{r}_2 f_x^{\text{KLI}}(\mathbf{r}_1, \mathbf{r}_2; \omega) |\varphi_k(\mathbf{r}_2)|^2 \right] \\ & - (\mathbf{r}_1 \leftrightarrow \mathbf{r}_4) - \sum_{kp}^{\text{occ}} \frac{|\varphi_k(\mathbf{r}_1)|^2}{\gamma(\mathbf{r}_1)} \frac{|\varphi_p(\mathbf{r}_4)|^2}{\gamma(\mathbf{r}_4)} \left[\frac{1}{2} \int d\mathbf{r}_2 d\mathbf{r}_3 \varphi_p(\mathbf{r}_2) \varphi_p(\mathbf{r}_3) v(\mathbf{r}_3, \mathbf{r}_2) \varphi_k(\mathbf{r}_2) \varphi_k(\mathbf{r}_3) \right] \end{aligned}$$

$$\begin{aligned}
 & + \int d\mathbf{r}_2 d\mathbf{r}_3 |\varphi_k(\mathbf{r}_2)|^2 f_x^{\text{KLI}}(\mathbf{r}_2, \mathbf{r}_3; \omega) |\varphi_p(\mathbf{r}_3)|^2 \Big] - \alpha_\varepsilon(\omega) \sum_k^{\text{occ}} \frac{|\varphi_k(\mathbf{r}_1)|^2}{\gamma(\mathbf{r}_1)} \frac{|\varphi_k(\mathbf{r}_4)|^2}{\gamma(\mathbf{r}_4)} \langle \varphi_k | D_x | \varphi_k \rangle \\
 & + \frac{\alpha_\varepsilon(\omega)}{2} \sum_k^{\text{occ}} \frac{|\varphi_k(\mathbf{r}_4)|^2}{\gamma(\mathbf{r}_4)} \left[v_x(\mathbf{r}_1) \frac{|\varphi_k(\mathbf{r}_1)|^2}{\gamma(\mathbf{r}_1)} - \frac{\varphi_k(\mathbf{r}_1)}{\gamma(\mathbf{r}_1)} \int d\mathbf{r}_2 \Sigma_x(\mathbf{r}_1, \mathbf{r}_2) \varphi_k(\mathbf{r}_2) \right] + (\mathbf{r}_1 \leftrightarrow \mathbf{r}_4). \quad (53)
 \end{aligned}$$

We note that the frequency dependence is not completely eliminated by the KLI-LHF approximations. Terms which behave as ω^2 remain. There will thus be a small violation of the f -sum rule, which can be traced to the fact that the KLI-LHF kernels are not obtained as functional derivatives of the corresponding potentials and hence the cancellation found in the exact equation [2] is incomplete. The frequency dependence appears in front of the self-energy terms and can thus enhance features related to such effects.

The KLI kernel is undetermined up to the addition of two functions $g_x(\mathbf{r}, \omega)$ and $g_x(\mathbf{r}', \omega)$, as in the case of the exact EXX kernel. In the previous section, we derived conditions that should be imposed on Eq. (37) in order to fix these functions. By performing a KLI approximation to the same equation, we find

$$\begin{aligned}
 0 = & \frac{1}{2} \frac{|\varphi_H(\mathbf{r}_1)|^2}{\gamma(\mathbf{r}_1)} v_x(\mathbf{r}_1) - \frac{\varphi_H(\mathbf{r}_1)}{\gamma(\mathbf{r}_1)} \int d\mathbf{r}_2 \Sigma_x(\mathbf{r}_1, \mathbf{r}_2) \varphi_H(\mathbf{r}_2) \\
 & + \int d\mathbf{r}_2 |\varphi_H(\mathbf{r}_2)|^2 f_x^{\text{KLI}}(\mathbf{r}_2, \mathbf{r}_1) \\
 & - \sum_k^{\text{occ}} \frac{|\varphi_k(\mathbf{r}_1)|^2}{\gamma(\mathbf{r}_1)} \left[\int d\mathbf{r}_2 d\mathbf{r}_3 |\varphi_H(\mathbf{r}_2)|^2 f_x^{\text{KLI}}(\mathbf{r}_2, \mathbf{r}_3) |\varphi_k(\mathbf{r}_3)|^2 \right. \\
 & \left. + \frac{1}{2} \int d\mathbf{r}_2 d\mathbf{r}_3 \varphi_k(\mathbf{r}_2) \varphi_k(\mathbf{r}_3) v(\mathbf{r}_2, \mathbf{r}_3) \varphi_H(\mathbf{r}_2) \varphi_H(\mathbf{r}_3) \right]. \quad (54)
 \end{aligned}$$

This condition together with

$$\begin{aligned}
 0 = & \int d\mathbf{r}_2 d\mathbf{r}_3 |\varphi_H(\mathbf{r}_2)|^2 f_x^{\text{KLI}}(\mathbf{r}_2, \mathbf{r}_3) |\varphi_H(\mathbf{r}_3)|^2 \\
 & + \frac{1}{2} \int d\mathbf{r}_2 d\mathbf{r}_3 |\varphi_H(\mathbf{r}_2)|^2 v(\mathbf{r}_2, \mathbf{r}_3) |\varphi_H(\mathbf{r}_3)|^2 \quad (55)
 \end{aligned}$$

arising from Eq. (23) allows one to remove all the terms containing the HOMO orbital in f_x^{DD} . At the same time, f_x^{KLI} is uniquely determined. Notice that we have not considered the frequency dependence here.

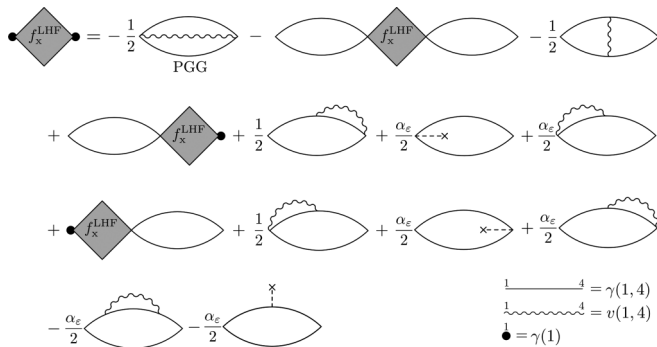


FIG. 2. Diagrammatic representation of the equation for the EXX kernel in the LHF approximation.

The discontinuity in the KLI approximation can also be determined as

$$\begin{aligned}
 g_x(\mathbf{r}_1) & = \frac{1}{2} \frac{|\varphi_L(\mathbf{r}_1)|^2}{\gamma(\mathbf{r}_1)} v_x(\mathbf{r}_1) - \frac{\varphi_L(\mathbf{r}_1)}{\gamma(\mathbf{r}_1)} \int d\mathbf{r}_2 \Sigma_x(\mathbf{r}_1, \mathbf{r}_2) \varphi_L(\mathbf{r}_2) \\
 & + \int d\mathbf{r}_2 |\varphi_L(\mathbf{r}_2)|^2 f_x^-(\mathbf{r}_2, \mathbf{r}_1) \\
 & - \sum_k \frac{|\varphi_k(\mathbf{r}_1)|^2}{\gamma(\mathbf{r}_1)} \left[\int d\mathbf{r}_2 d\mathbf{r}_3 |\varphi_L(\mathbf{r}_2)|^2 f_x^-(\mathbf{r}_2, \mathbf{r}_3) |\varphi_k(\mathbf{r}_3)|^2 \right. \\
 & - \int d\mathbf{r}_3 g_x(\mathbf{r}_3) |\varphi_k(\mathbf{r}_3)|^2 \\
 & \left. + \frac{1}{2} \int d\mathbf{r}_2 d\mathbf{r}_3 \varphi_k(\mathbf{r}_2) \varphi_k(\mathbf{r}_3) v(\mathbf{r}_2, \mathbf{r}_3) \varphi_L(\mathbf{r}_2) \varphi_L(\mathbf{r}_3) \right]. \quad (56)
 \end{aligned}$$

This equation shows that the sum of the additional terms beyond the PGG can be seen as the explicit inclusion of the discontinuity.

We will now briefly discuss how the KLI equations are solved in practice. As suggested in Ref. [33], the KLI potential can be determined by first multiplying Eq. (47) with $|\varphi_k(\mathbf{r}_1)|^2$, where k is occupied, and then integrate with respect to \mathbf{r}_1 . This leads to a matrix equation determining the constants $\int |\varphi_k|^2 v_x^{\text{KLI}}$, appearing on the right-hand side of Eq. (47). When these constants are known, $v_x^{\text{KLI}}(\mathbf{r}_1)$ is easily calculated. The same idea is here used for calculating the KLI kernel [Eqs. (52) and (53)]. Hence, we first multiply with $|\varphi_k(\mathbf{r}_1)|^2$ and $|\varphi_p(\mathbf{r}_4)|^2$ and then integrate with respect to \mathbf{r}_1 and \mathbf{r}_4 . This allows us to calculate the constants $\int |\varphi_k|^2 f_x^{\text{KLI}} |\varphi_p|^2$ via a matrix equation. With these constants known, it is easy to derive another equation for the vectors $\int d\mathbf{r}_2 f_x^{\text{KLI}}(\mathbf{r}_1, \mathbf{r}_2; \omega) |\varphi_p(\mathbf{r}_2)|^2$, which together with the constants allows us to calculate $f_x^{\text{KLI}}(\mathbf{r}_1, \mathbf{r}_2; \omega)$.

V. NUMERICAL RESULTS AND ANALYSIS

In this section, we present numerical results for 1D soft-Coulomb systems. Such model systems are often used to study qualitative features similar to those arising in three-dimensional (3D) molecules. In this model, the Coulomb interaction is “softened” such that the electron-electron interaction is given by $1/\sqrt{(x_1 - x_2)^2 + 1}$, where x_1 and x_2 are the coordinates of electrons 1 and 2, respectively. Also, the nuclear potentials are softened and given by $1/\sqrt{(x_1 - Q)^2 + 1}$, where Q is the position of the nucleus.

All calculations have been performed using cubic splines as basis functions, uniformly distributed along the x axis. Details on the numerical approach can be found in Ref. [50].

A. Diatomic molecules at dissociation

A molecule that dissociates is one of the hardest systems to describe within density-functional theory (DFT). This is especially true when the molecule consists of open-shell atoms and has covalent bonds. In this case, the system is strongly correlated and can not be described with an exchange-only theory. Applying the EXX approximation leads to largely underestimated total energies and fractionally charged dissociation fragments. The latter, so-called delocalization problem is due to a missing derivative discontinuity at *odd* integer particle numbers in the EXX functional.

Molecules composed of closed-shell atoms can also be difficult to describe at dissociation using standard functionals giving rise to similar fractional charge problems. In the case of closed-shell fragments, the functional needs to have a derivative discontinuity at *even* integers. As we have seen in the previous section, such a discontinuity is contained already at the EXX level. This allows us to study the fractional charge and discontinuity problem within the EXX functional.

In order to see when the discontinuity is needed for describing a stretched molecule, one can study its constituent atoms independently. Since the unoccupied KS levels have no physical significance, it may happen that the KS affinity of one of the atoms is larger than the ionization energy of the other atom. Enforcing the Aufbau principle, a step over the atom with the large affinity is needed when the atoms are described as a combined system at infinite separation. An example of such a system is the model HeBe^{2+} molecule, in which the nuclear strength of the He nucleus is set to 2.5. This gives an ionization energy $I = 1.147$ and a KS affinity $A_s = 0.494$. The Be^{2+} nucleus is set to 4.5 giving $I = 2.836$ and $A_s = 1.673$. We now see that A_s of the Be^{2+} is larger than I of the He atom and a step of minimum 0.526 is required at infinite separation.

Figure 3 shows the EXX, the KLI, and the Slater potentials of the HeBe^{2+} system at different separation R . Both the EXX and the KLI have a step as predicted, being somewhat sharper in the EXX. The step ensures integer charges on the atoms,

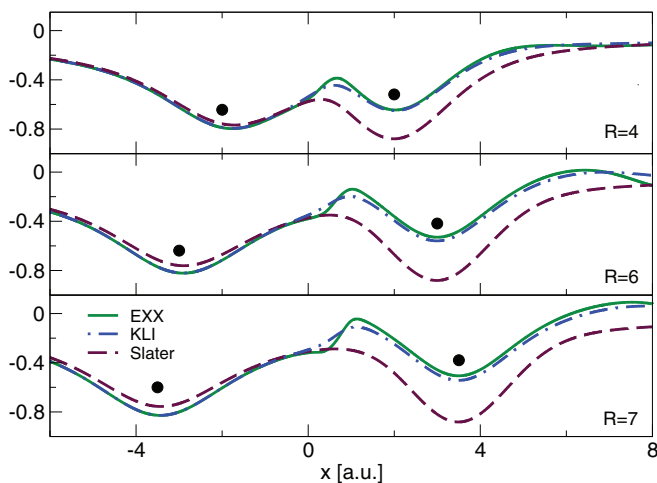


FIG. 3. (Color online) The black circles show the position of two atoms at different separations R . The left with nuclear strength 2.5 and the right 4.5. In total, there are four electrons. Due to the missing step in the PGG approximation, the density dissociates with fractional charges on the atoms.

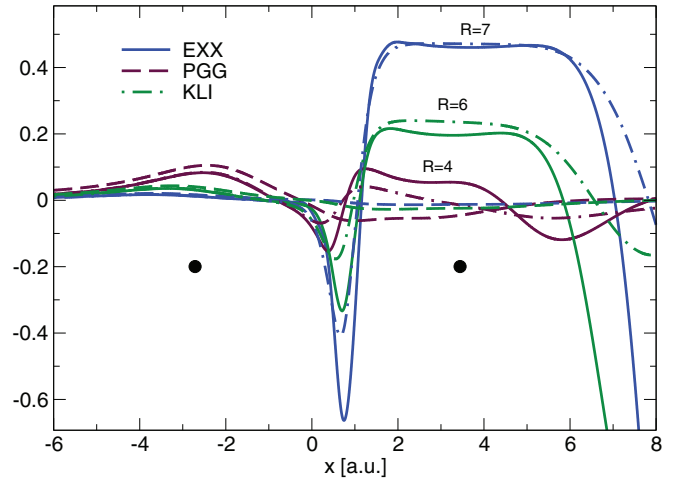


FIG. 4. (Color online) The same systems as in Fig. 3. The quantity $\int d\mathbf{r}' \Phi_q(\mathbf{r}') f_x(\mathbf{r}', \mathbf{r}, \omega = 0)$ is plotted where Φ_q is the excitation function of the HOMO-LUMO excitation being a charge-transfer excitation from left to right.

something which we have also verified numerically. The Slater potential which lacks the step gives an excess of 0.1 charges on the Be^{2+} atom. At large separation, the difference between the Slater and the KLI-EXX potentials is almost exactly a constant over the Be^{2+} atom showing the close relation between the second term of Eq. (47) and the discontinuity.

In Fig. 4, the kernel of the same system is shown. The quantity that is plotted is

$$\int d\mathbf{r}' \Phi_q(\mathbf{r}') f_x(\mathbf{r}', \mathbf{r}, \omega = 0), \quad (57)$$

which is equal to the induced change in v_x given that the density change is equal to Φ_q . Here, Φ_q is set to the excitation function corresponding to the HOMO-LUMO transition thus representing a charge-transfer excitation. We see that even though Φ_q is vanishingly small, due to the exponentially decreasing overlap of the HOMO and at the LUMO orbitals, the kernel shows large structures in terms of peaks and a plateau that grows with separation. This structure which is missing in the PGG kernel comes entirely from f_x^{DD} which contains the effects of the discontinuity. In the next section, we will see that the discontinuity has very similar shape. Integrating Eq. (57) with another Φ_q gives $\langle \Phi_q | f_x | \Phi_q \rangle$ which is proportional to the correction to the charge-transfer excitation energy in the adiabatic single-pole approximation. While in the PGG this correction quickly tends to zero, it grows with separation in both EXX and KLI. On the other hand, the matrix element of f_x calculated with a Φ_q of an excitation localized on the Be atom converges to the value of the isolated atom, unaffected by the discontinuity. Thus, *locally* the discontinuity merely adds an irrelevant function g_{xc} to the kernel. We will discuss excitation energies more in Sec. III D.

B. Ensemble v_x and f_x

As discussed previously, the property a functional needs to have in order to produce a step in v_{xc} in a stretched molecule is the derivative discontinuity. The discontinuity of a given functional can be studied if the domain of densities is extended

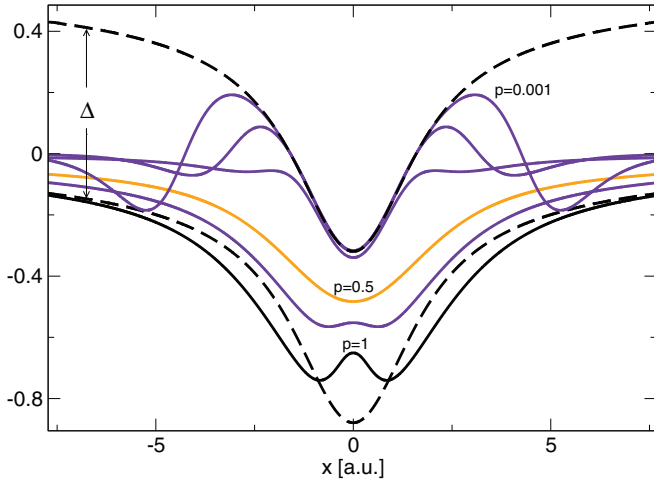


FIG. 5. (Color online) The ensemble EXX potential of Be^{2+} for different values of p such that $4 \leq N \leq 2$. The dashed curves are obtained by calculating the two-electron potential from the two different limits $N \rightarrow 2^\pm$.

to ensemble densities of the kind discussed in Secs. II A and II B. In the following, we will calculate the ensemble v_x and f_x and their discontinuities and relate them to the structures seen in the stretched molecules.

Equations (36) and (37) were generalized to ensembles as discussed in Sec. III and solved numerically together with the conditions of Eqs. (39) and (40) (before the limit $N \rightarrow N_0^+$ is taken). The discontinuities were also calculated [Eqs. (43) and (44)]. Figure 5 shows the EXX potential of Be^{2+} for different values of p . By varying p between 0 and 1, the number of particles change between 2 and 4. The dashed curves represent v_x for two electrons but calculated from the two different limits $N \rightarrow 2^+$ and $N \rightarrow 2^-$. The difference between the curves is the discontinuity Δ_x , exactly given by Eq. (43). This was also verified numerically. For $p < 1$, we find a step in v_x that becomes sharper and sharper and moves further away from the center as $p \rightarrow 0^+$. This structure is similar to the structure over the Be^{2+} atom in the molecule for EXX and KLI, thus confirming the close relation between the discontinuity of the ensemble potential and the step during dissociation.

In Fig. 6 we have plotted the corresponding static ensemble kernel

$$F_H(\mathbf{r}) = \int d\mathbf{r}' f_x(\mathbf{r}, \mathbf{r}') |\varphi_H(\mathbf{r}')|^2 \quad (58)$$

and we notice that

$$F_H^+(\mathbf{r}) = \int d\mathbf{r}' f_x^-(\mathbf{r}, \mathbf{r}') |\varphi_H(\mathbf{r}')|^2 + \int d\mathbf{r}' g_x(\mathbf{r}') |\varphi_H(\mathbf{r}')|^2 + g_x(\mathbf{r}). \quad (59)$$

The dashed lines correspond to the kernel calculated from the two different limits $N \rightarrow 2^+$ and $N \rightarrow 2^-$. Here, we see a rather large difference which amounts to the discontinuity g_x and the constant $\int g_x |\varphi_H|^2$ according to Eq. (59). The diverging behavior that was deduced from the analysis in Sec. II B is thus confirmed for the EXX kernel. Before the limit is reached, the ensemble kernel displays sharp peaks and a plateaulike structure very similar to those observed in the stretched molecule of the EXX and KLI. The fact that

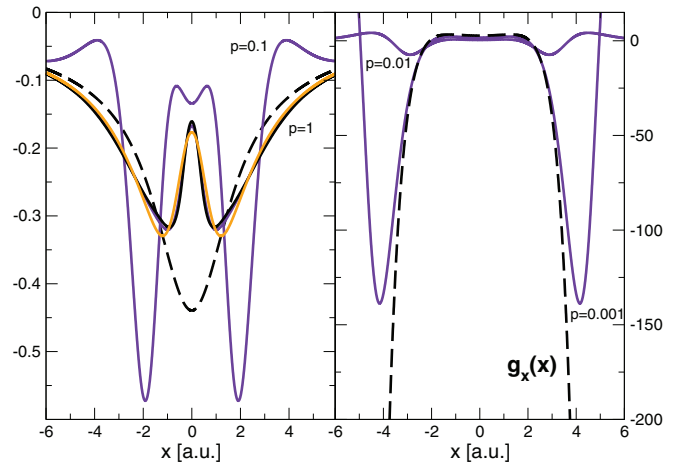


FIG. 6. (Color online) The ensemble EXX kernel of Be^{2+} for different values of p such that $4 \leq N \leq 2$. Left panel shows $p = 1, 0.8, 0.5, 0.1$ and the right panel shows $p = 0.01, 0.001$. The dashed curves in the different panels are obtained by calculating the two-electron potential from the two different limits $N \rightarrow 2^\pm$.

the discontinuity diverges is exactly what allows the kernel of the combined system to capture long-range charge-transfer excitations. Figure 7 shows the discontinuity at $\omega = 0, 0.5$ (below the first excitation energy), 1.0, and at $\omega = 1.2$. The discontinuity obtained from Eq. (40) contains poles at the energy differences between the LUMO and the rest of the unoccupied and occupied states (see inset of Fig. 7). Only the LUMO to the occupied states corresponds to KS excitation energies contained also in χ_s . We see that the frequency changes the strength of the divergency of the discontinuity. This is expected since the same kernel has to describe all charge-transfer states which all have different excitation functions decaying at different rates.

C. Field-counteracting effect

In Refs. [51,52] it was found that when applying a weak electric field to a chain of hydrogen molecules the EXX

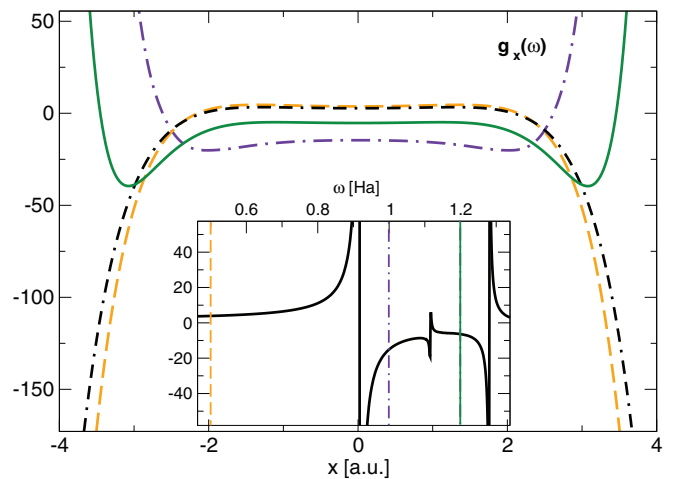


FIG. 7. (Color online) The discontinuity of the EXX kernel calculated at different frequencies. The inset shows $\int |\varphi|^2 f_x(\omega) |\varphi|^2$ and at which frequency the discontinuity is evaluated.

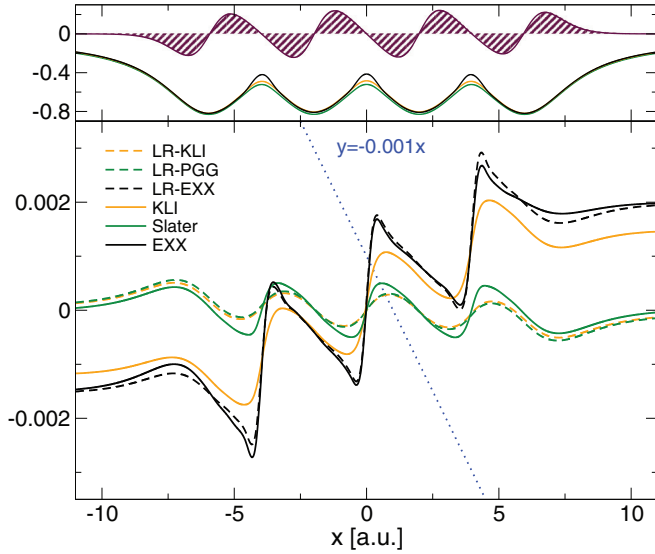


FIG. 8. (Color online) Upper panel: The EXX potential (EXX, PGG, and KLI) of a chain of four H_2 molecules. The density difference obtained when applying a linear potential is shown as the shaded top curve. Lower panel: The EXX potential differences when applying a linear potential as calculated from the kernel (dashed lines) and as the difference between two independent self-consistent KS calculations (solid lines). Blue dotted curve is the applied linear potential.

potential exhibits a step structure, counteracting the applied field. It was then shown that calculating the polarizability by taking the difference between densities with and without field, the values were strongly dependent of this property. The field-counteracting effect is an exchange effect when the constituent molecules are closed shell as in the case of a H_2 chain. This allows us here to study this effect and give it a perspective in terms of the discontinuity of the kernel.

We have studied a chain of four H_2 molecules. Figure 8 (upper panel) shows the PGG-KLI-EXX potentials of this chain as well as the density difference obtained by applying a weak constant electric field with potential $V = 0.001x$. In the lower panel, the EXX potential differences (Δv_x) are displayed with full lines. We clearly see a step structure counteracting the applied field in the EXX and the KLI. The KLI somewhat underestimates the incline and the PGG misses it completely, which is related to the missing discontinuity in the Slater potential.

An alternative way to calculate the potential differences is to use

$$\delta v_{xc}(\mathbf{r}) = \int d\mathbf{r}' f_{xc}(\mathbf{r}, \mathbf{r}') \delta n(\mathbf{r}'), \quad (60)$$

exact when the applied field is infinitesimally small. The results can be found as the dashed curves in Fig. 8. Note here that only the full EXX is expected to give an identical result to the potential difference calculations since only in that case does the kernel represent the true functional derivative. The KLI gives a result very similar to PGG. This has to do with the fact that the system is symmetric and was pointed out already in Ref. [34].

Figure 9 shows the same curves as in the case of the H_2 chain but for the asymmetric $HeBe^{2+}$ system. Again, a step is

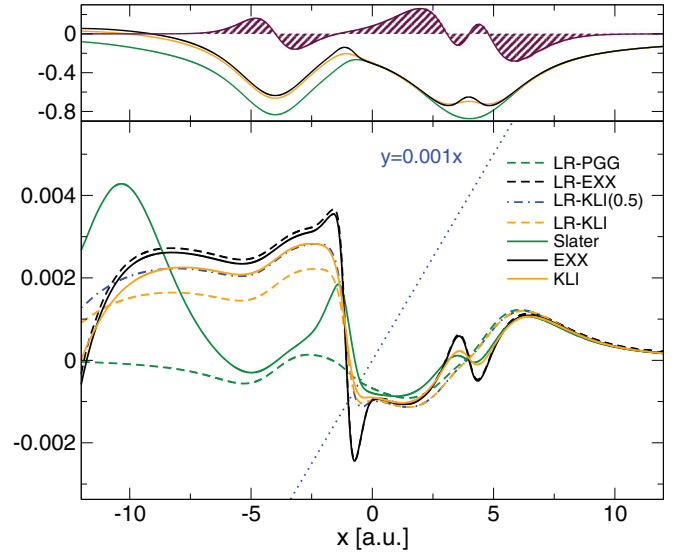


FIG. 9. (Color online) Upper panel: The EXX potential (EXX, PGG and KLI) of a $He-Be^{2+}$ dimer. The density difference obtained when applying a linear potential is shown as the shaded top curve. Lower panel: The EXX potential differences when applying a linear potential as calculated from the kernel (dashed lines) and as the difference between two independent self-consistent KS calculations (solid lines). The dashed-dotted curve is obtained by setting $\alpha = 0.5$. Blue dotted curve is the applied linear potential.

found in EXX and KLI but missing in PGG. We also see that it is possible to tune the KLI result by changing the frequency such that the response calculation coincides with the potential differences. The frequency dependence of the KLI can thus change the strength of the discontinuity. It is clear that the step structures found in v_x can be seen as a consequence of the discontinuity in f_x .

D. Excitation energies

The LR-TDDFT equation is often compared to the Bethe-Salpeter equation (BSE). The BSE contains a four-point kernel and an interacting Green's function as input, whereas the LR-TDDFT equation requires only a two-point kernel and a noninteracting KS Green's function as input. For molecular valence excitations, a KS Green's function can be a better starting point than an interacting Green's function. The latter contains energy differences with respect to addition and removal energies that need to be corrected with the particle-hole interaction, and part of this is already contained in the KS excitation energies due to the $1/R$ behavior of the KS potential. There are, however, excitations for which a full G serves as a better starting point. Among those excitations belong long-range charge-transfer and inner-shell excitations. It is therefore not surprising that a theory based on replacing the interacting G with a noninteracting G_s has difficulties in accurately capturing these excitations [12,16]. We will see examples of this problem shortly, but before that we will investigate the single-pole approximation (SPA) within LR-TDDFT. The SPA ignores off-diagonal elements in the Casida matrix and expands the diagonal elements around the

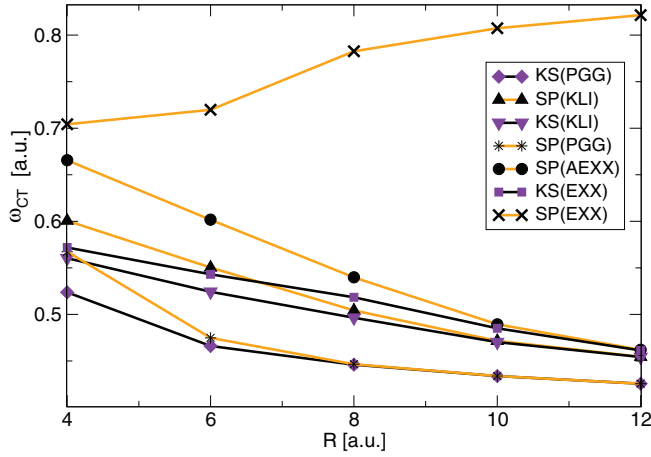


FIG. 10. (Color online) The first charge-transfer excitation energy for the system in Fig. 11 evaluated in the SPA. Only the fully frequency-dependent kernel is able to give a correction to the KS eigenvalue difference at large R .

KS excitation energies. One obtains

$$\Omega_q = \omega_q + 2\langle\Phi_q|v + f_x(\omega_q)|\Phi_q\rangle. \quad (61)$$

One can also show that this approximation yields excitation energies identical to those obtained from first-order Görling-Levy perturbation theory [53,54]. Within the SPA, we can thus calculate excitation energies not subjected to errors that can arise when carrying out improper partial summations.

Figure 10 shows the first charge-transfer excitation energy of the HeBe^{2+} system. We have decreased the charge on the Be^{2+} atom to 3 a.u., in order to remove the step in v_x . In this way, the KS excitation energies are not artificially shifted and the effect of the discontinuity comes entirely from the kernel (see Fig. 11). In the SPA, we see that only the fully frequency-dependent kernel is able to give a finite correction to the KS excitation energy in the dissociation limit. Figure 11 indeed shows that the step is strongly enhanced at finite frequency. The adiabatic approximation works rather well for small R

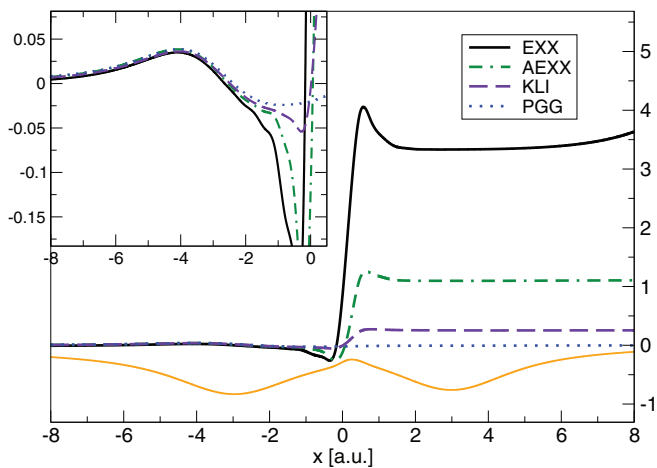


FIG. 11. (Color online) The kernel of a stretched HeBe^{2+} molecule for which the charge on the Be^{2+} atom is set to 3 a.u. In this case, the step in v_x vanishes in the dissociation limit but the step in f_x grows and eventually diverges.

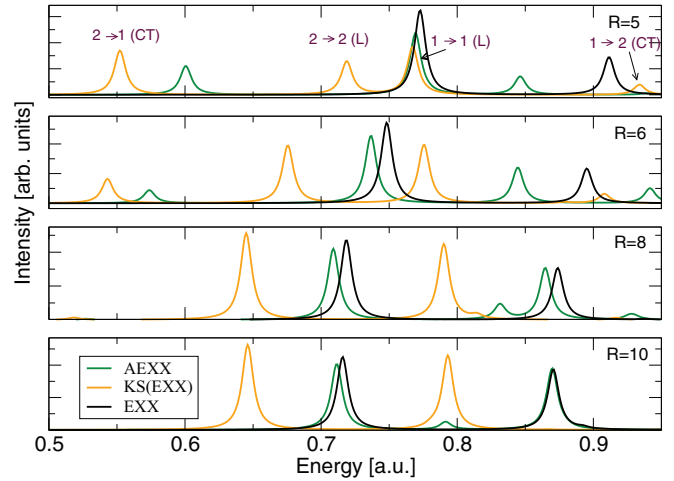


FIG. 12. (Color online) The spectrum of HeBe^{2+} at different separation R . The KS charge-transfer (CT) and the local (L) excitations are identified at $R = 5$.

but then deviates more and more and finally joins the KS eigenvalue difference. The KLI kernel behaves similarly to the AEEX and the PGG is seen to even more rapidly converge to the KS energy.

If we solve the full LR-TDDFT equation, we find the results of Fig. 12. The first two charge-transfer (CT) excitations as well as one local (L) excitation on each atom are identified. With the AEEX we find the same number of peaks but shifted to higher energies. The charge-transfer excitations are also here seen to reduce to the KS eigenvalue differences in the dissociation limit, even slightly faster than in the SPA. The local excitations are converging to the values found for the isolated atoms. Since there are only two electrons on each atom, the AEEX and the full EXX are identical in the dissociation limit with respect to local excitations. This is indeed also what we see at $R = 10$, which confirms the fact that the large step in f_x (Fig. 11) does not influence the local excitations. The effect of the frequency dependence on the CT excitations appears to be to remove them completely from the spectrum. A smeared structure can be seen for $R = 5$ at $\omega = 0.6$, but if we reduce the δ width this structure becomes even more broadened, which suggests that this is not a proper excitation. A similar disappearance of peaks happens in the case of inner-shell excitations as we will now discuss.

To investigate inner-shell transitions, we study a four-electron 1D atom with the nuclear charge set to 4.5 a.u. The KS eigenvalue difference for the first inner-shell transition is around 1.3 a.u. In the SPA, the different approximations give a correction of 0.1624 (EXX), 0.0132 (AEEX), 0.0152 (KLI), -0.001755 (PGG). PGG is the only approximation that gives a negative contribution, which also is very small. KLI and AEEX gives a correction an order of magnitude larger than PGG and the frequency-dependent EXX yet another order of magnitude. Clearly, a frequency dependence is important in this case and this is true for all inner-shell excitation energies. The fact that PGG differs so much from KLI also suggests that the discontinuity is of importance for these excitations.

If we instead solve the full LR-TDDFT equations with the EXX kernel we find that all inner-shell excitations are missing

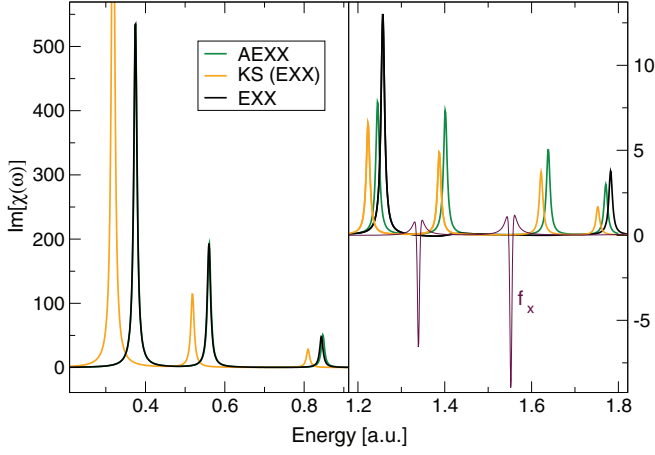


FIG. 13. (Color online) Spectrum of a four-electron 1D Be atom. At low energy, the EXX and AEXX are very similar but start to differ at higher energies. In the EXX, all inner-shell excitations are missing due to the double-pole structure that can be found in the kernel close to every inner-shell excitation.

from the spectra (Fig. 13). This fact was already discovered in Ref. [12] and here we see that also 1D systems exhibit this behavior. The reason for this is the double-pole structure of f_x which in turn is related to the double inversion of the KS response function, which has zero eigenvalues at these frequencies. Double poles can lead to a noncausal response function with poles symmetrically located in the upper and lower halves of the complex plane as shown in Ref. [12]. The exact kernel must have a strong frequency dependence at these energies, but further analysis shows that a single-pole structure is the correct one.

Figure 13 also shows the result obtained using the AEXX, showing that at lower energies EXX and AEXX are very close for this system.

VI. CONCLUSIONS

In this paper, we have analyzed the integer discontinuity of the XC kernel by extending its domain of densities to ensemble densities that integrate to noninteger particle numbers. It was found that in order to completely determine the discontinuity the ensemble densities had to be general enough to allow for changes of particle numbers in time.

The discontinuity of the ensemble kernel was evaluated showing a diverging spatial dependence and a pole structure in the frequency. Such strong features have, however, no effect on the calculated spectra at integer particle numbers. On the other hand, in a combined system, such as a stretched molecule, where the discontinuity shows up on only a part of the system, the discontinuity can have a large effect. This implies that locally such behavior does not affect the excitations, but for excitations involving transfer of charge the effect can be large.

A numerical study was performed within the EXX approximation. Two different approximations to the EXX kernel were derived: the PGG approximation which has been used previously and a new KLI type of approximation solved numerically. The KLI approximation captures explicitly the discontinuity of the full adiabatic EXX approximation. It was

also shown that an additional term in the KLI approximation could be used to tune the strength of the discontinuity.

By comparing the PGG, KLI, AEXX, and EXX we were able to identify properties that are dependent on the discontinuity of the functional. For example, the field-counteracting effect in a molecule chain can be seen as a consequence of the discontinuity of the kernel. For charge-transfer excitations, the discontinuity provides the diverging behavior needed to compensate for the vanishing overlap of the KS orbitals. Also, local inner-shell excitations are strongly modified when incorporating the discontinuity. It was also shown that none of the approximations studied here have the proper frequency dependence to fully account for these excitations. There is thus a need to go beyond exact exchange for accurately calculating spectral properties within TDDFT.

APPENDIX: LHF APPROXIMATION TO $\chi_s f_x \chi_s$

We here present the full derivation of $R(\mathbf{r}_1, \mathbf{r}_4; \omega)$ in Eq. (49). Within TDEXX, the right-hand side of Eq. (37) consists of a vertex term [first term in Eq. (37) or third diagram of Fig. 1] and self-energy terms.

After performing the frequency integrals, the vertex term R_V can be written as

$$R_V = 2 \sum_{kpsr} \varphi_s(\mathbf{r}_1) \varphi_r^*(\mathbf{r}_1) \varphi_p(\mathbf{r}_4) \varphi_k^*(\mathbf{r}_4) \langle sp | v | kr \rangle \times \left[\frac{(1 - n_s) n_r (1 - n_p) n_k (2\omega^2 + 2\varepsilon_{sr} \varepsilon_{kp})}{(\omega^2 - \varepsilon_{sr}^2)(\omega^2 - \varepsilon_{kp}^2)} - \frac{(1 - n_s) n_r (1 - n_k) n_p (2\omega^2 + 2\varepsilon_{sr} \varepsilon_{kp})}{(\omega^2 - \varepsilon_{sr}^2)(\omega^2 - \varepsilon_{kp}^2)} \right], \quad (\text{A1})$$

where k , p , s , and r run over the KS states. In the CEDA the eigenvalue differences between occupied and unoccupied are all set to the same value $\varepsilon = \varepsilon_{kk'} = \varepsilon_k - \varepsilon_{k'}$. Using $\sum_k \varphi_k(\mathbf{r}_1) \varphi_k^*(\mathbf{r}_2) = \delta(\mathbf{r}_1, \mathbf{r}_2)$, the two terms above reduce to

$$V_1 = \frac{4}{\omega^2 - \varepsilon^2} \left[\gamma^2(\mathbf{r}_4, \mathbf{r}_1) v(\mathbf{r}_4, \mathbf{r}_1) + \int d\mathbf{r}_2 d\mathbf{r}_3 \gamma(\mathbf{r}_4, \mathbf{r}_2) \gamma(\mathbf{r}_4, \mathbf{r}_3) v(\mathbf{r}_3, \mathbf{r}_2) \times \gamma(\mathbf{r}_2, \mathbf{r}_1) \gamma(\mathbf{r}_3, \mathbf{r}_1) + \int d\mathbf{r}_2 \Sigma_x(\mathbf{r}_1, \mathbf{r}_2) \gamma(\mathbf{r}_2, \mathbf{r}_4) \gamma(\mathbf{r}_4, \mathbf{r}_1) + \int d\mathbf{r}_2 \Sigma_x(\mathbf{r}_4, \mathbf{r}_2) \gamma(\mathbf{r}_2, \mathbf{r}_1) \gamma(\mathbf{r}_4, \mathbf{r}_1) \right] \quad (\text{A2})$$

and

$$V_2 = -4 \frac{\omega^2 + \varepsilon^2}{(\omega^2 - \varepsilon^2)(\omega^2 - \varepsilon^2)} \left[\int d\mathbf{r}_2 d\mathbf{r}_3 \gamma(\mathbf{r}_4, \mathbf{r}_2) \times \gamma(\mathbf{r}_4, \mathbf{r}_3) v(\mathbf{r}_3, \mathbf{r}_2) \gamma(\mathbf{r}_2, \mathbf{r}_1) \gamma(\mathbf{r}_3, \mathbf{r}_1) + \int d\mathbf{r}_2 \Sigma_x(\mathbf{r}_1, \mathbf{r}_2) \gamma(\mathbf{r}_2, \mathbf{r}_4) \gamma(\mathbf{r}_4, \mathbf{r}_1) + \int d\mathbf{r}_2 \Sigma_x(\mathbf{r}_4, \mathbf{r}_2) \gamma(\mathbf{r}_2, \mathbf{r}_1) \gamma(\mathbf{r}_4, \mathbf{r}_1) - \int d\mathbf{r}_2 \Sigma_x(\mathbf{r}_1, \mathbf{r}_2) \gamma(\mathbf{r}_2, \mathbf{r}_4) \delta(\mathbf{r}_4, \mathbf{r}_1) \right]. \quad (\text{A3})$$

The four self-energy terms are given by

$$\begin{aligned}
 & R_{\Sigma_1} + R_{\Sigma_2} + R_{v_x,1} + R_{v_x,2} \\
 &= 4 \sum_{psr} [\langle p|v_x|r\rangle - \langle p|\Sigma_x|r\rangle] \varphi_s^*(\mathbf{r}_4) \varphi_p(\mathbf{r}_4) \varphi_s(\mathbf{r}_1) \varphi_r^*(\mathbf{r}_1) \left\{ \frac{n_p n_r (1-n_s)(\omega^2 + \varepsilon_{sp} \varepsilon_{sr})}{(\omega^2 - \varepsilon_{sp}^2)(\omega^2 - \varepsilon_{sr}^2)} + \frac{n_p(1-n_r)n_s \varepsilon_{sr}}{\varepsilon_{rp}(\omega^2 - \varepsilon_{sr}^2)} \right. \\
 &\quad \left. - \frac{n_p(1-n_r)(1-n_s)\varepsilon_{sp}}{\varepsilon_{pr}(\omega^2 - \varepsilon_{sp}^2)} + \frac{(1-n_p)n_r n_s \varepsilon_{sp}}{\varepsilon_{pr}(\omega^2 - \varepsilon_{sp}^2)} - \frac{(1-n_p)n_r(1-n_s)\varepsilon_{sr}}{\varepsilon_{rp}(\omega^2 - \varepsilon_{sr}^2)} - \frac{(1-n_p)(1-n_r)n_s(\omega^2 + \varepsilon_{sp} \varepsilon_{sr})}{(\omega^2 - \varepsilon_{sp}^2)(\omega^2 - \varepsilon_{sr}^2)} \right\}. \quad (\text{A4})
 \end{aligned}$$

After the CEDA, these six terms reduce to four:

$$T_1 = 4 \frac{\omega^2 + \varepsilon^2}{(\omega^2 - \varepsilon^2)(\omega^2 - \varepsilon^2)} \left[\int d\mathbf{r}_2 d\mathbf{r}_3 \gamma(\mathbf{r}_1, \mathbf{r}_2) D_x(\mathbf{r}_2, \mathbf{r}_3) \gamma(\mathbf{r}_3, \mathbf{r}_4) [\delta(\mathbf{r}_1, \mathbf{r}_4) - \gamma(\mathbf{r}_4, \mathbf{r}_1)] \right], \quad (\text{A5})$$

$$T_2 = T_3 = -4 \frac{\gamma(\mathbf{r}_4, \mathbf{r}_1)}{\omega^2 - \varepsilon^2} \left[\int d\mathbf{r}_2 D_x(\mathbf{r}_1, \mathbf{r}_2) \gamma(\mathbf{r}_2, \mathbf{r}_4) - \int d\mathbf{r}_2 d\mathbf{r}_3 \gamma(\mathbf{r}_1, \mathbf{r}_2) D_x(\mathbf{r}_2, \mathbf{r}_3) \gamma(\mathbf{r}_3, \mathbf{r}_4) \right], \quad (\text{A6})$$

$$T_4 = T_5 = -4 \frac{\gamma(\mathbf{r}_4, \mathbf{r}_1)}{\omega^2 - \varepsilon^2} \left[\int d\mathbf{r}_2 D_x(\mathbf{r}_4, \mathbf{r}_2) \gamma(\mathbf{r}_2, \mathbf{r}_1) - \int d\mathbf{r}_2 d\mathbf{r}_3 \gamma(\mathbf{r}_1, \mathbf{r}_2) D_x(\mathbf{r}_2, \mathbf{r}_3) \gamma(\mathbf{r}_3, \mathbf{r}_4) \right], \quad (\text{A7})$$

$$\begin{aligned}
 T_6 = & -\frac{\omega^2 + \varepsilon^2}{(\omega^2 - \varepsilon^2)(\omega^2 - \varepsilon^2)} \gamma(\mathbf{r}_4, \mathbf{r}_1) \left[D_x(\mathbf{r}_1, \mathbf{r}_4) + \int d\mathbf{r}_2 d\mathbf{r}_3 \gamma(\mathbf{r}_1, \mathbf{r}_2) D_x(\mathbf{r}_2, \mathbf{r}_3) \gamma(\mathbf{r}_3, \mathbf{r}_4) - \int d\mathbf{r}_2 \gamma(\mathbf{r}_1, \mathbf{r}_2) D_x(\mathbf{r}_2, \mathbf{r}_4) \right. \\
 & \left. - \int d\mathbf{r}_2 D_x(\mathbf{r}_1, \mathbf{r}_2) \gamma(\mathbf{r}_2, \mathbf{r}_4) \right]. \quad (\text{A8})
 \end{aligned}$$

When we sum all terms, we find that the terms containing the $\delta(\mathbf{r}_1, \mathbf{r}_4)$ factor cancel by virtue of Eq. (46). The final result is presented in Eq. (49).

[1] C. A. Ullrich, *Time-Dependent Density Functional Theory* (Oxford University Press, Oxford, UK, 2012).
 [2] M. Hellgren and U. von Barth, *Phys. Rev. B* **78**, 115107 (2008).
 [3] M. Hellgren and U. von Barth, *J. Chem. Phys.* **132**, 044101 (2010).
 [4] A. Hesselmann and A. Görling, *Mol. Phys.* **108**, 359 (2010).
 [5] T. Gould and J. F. Dobson, *Phys. Rev. A* **85**, 062504 (2012).
 [6] T. Olsen and K. S. Thygesen, *Phys. Rev. B* **86**, 081103 (2012).
 [7] H. Eshuis, J. E. Bates, and F. Furche, *Theor. Chem. Acc.* **131**, 1 (2012).
 [8] E. Runge and E. K. U. Gross, *Phys. Rev. Lett.* **52**, 997 (1984).
 [9] E. K. U. Gross and W. Kohn, *Phys. Rev. Lett.* **55**, 2850 (1985).
 [10] M. Stener, P. Decleva, and A. Lisini, *J. Phys. B: At., Mol. Opt. Phys.* **28**, 4973 (1995).
 [11] M. Stener, P. Decleva, and A. Görling, *J. Chem. Phys.* **114**, 7816 (2001).
 [12] M. Hellgren and U. von Barth, *J. Chem. Phys.* **131**, 044110 (2009).
 [13] M. Lein, E. K. U. Gross, and J. P. Perdew, *Phys. Rev. B* **61**, 13431 (2000).
 [14] N. T. Maitra, F. Zhang, R. J. Cave, and K. Burke, *J. Chem. Phys.* **120**, 5932 (2004).
 [15] N. T. Maitra and D. G. Tempel, *J. Chem. Phys.* **125**, 184111 (2006).
 [16] M. Hellgren and E. K. U. Gross, *Phys. Rev. A* **85**, 022514 (2012).
 [17] J. P. Perdew, R. G. Parr, M. Levy, and J. L. Balduz, *Phys. Rev. Lett.* **49**, 1691 (1982).
 [18] J. P. Perdew, in *Density Functional Methods in Physics*, edited by R. M. Dreizler and J. da Providencia (Plenum, New York, 1985).
 [19] A. Makmal, S. Kümmel, and L. Kronik, *Phys. Rev. A* **83**, 062512 (2011).
 [20] P. Elliott, J. I. Fuks, A. Rubio, and N. T. Maitra, *Phys. Rev. Lett.* **109**, 266404 (2012).
 [21] S. Kurth, G. Stefanucci, E. Khosravi, C. Verdozzi, and E. K. U. Gross, *Phys. Rev. Lett.* **104**, 236801 (2010).
 [22] M. Lein and S. Kümmel, *Phys. Rev. Lett.* **94**, 143003 (2005).
 [23] M. Petersilka, U. J. Gossmann, and E. K. U. Gross, *Phys. Rev. Lett.* **76**, 1212 (1996).
 [24] M. Grüning, A. Marini, and A. Rubio, *J. Chem. Phys.* **124**, 154108 (2006).
 [25] I. V. Tokatly and O. Pankratov, *Phys. Rev. Lett.* **86**, 2078 (2001).
 [26] D. J. Tozer, *J. Chem. Phys.* **119**, 12697 (2003).
 [27] U. von Barth, N. E. Dahlen, R. van Leeuwen, and G. Stefanucci, *Phys. Rev. B* **72**, 235109 (2005).
 [28] M. E. Casida, *Phys. Rev. A* **51**, 2005 (1995).
 [29] Y.-H. Kim and A. Görling, *Phys. Rev. B* **66**, 035114 (2002).
 [30] A. Hesselmann and A. Görling, *Mol. Phys.* **109**, 2473 (2011).
 [31] A. Hesselmann and A. Görling, *Phys. Rev. Lett.* **106**, 093001 (2011).
 [32] M. Mundt and S. Kümmel, *Phys. Rev. Lett.* **95**, 203004 (2005).
 [33] J. B. Krieger, Y. Li, and G. J. Iafrate, *Phys. Rev. A* **45**, 101 (1992).
 [34] O. V. Gritsenko and E. J. Baerends, *Phys. Rev. A* **64**, 042506 (2001).

- [35] M. E. Casida, in *Recent Developments and Applications of Modern Density Functional Theory*, edited by J. M. Seminario (Elsevier, Amsterdam, 1996).
- [36] J. P. Perdew and M. Levy, *Phys. Rev. B* **56**, 16021 (1997).
- [37] M. Hellgren and E. K. U. Gross, *J. Chem. Phys.* **136**, 114102 (2012).
- [38] A. J. Cohen, P. Mori-Sanchez, and W. Yang, *Science* **321**, 792 (2008).
- [39] P. Mori-Sanchez, A. J. Cohen, and W. Yang, *Phys. Rev. Lett.* **102**, 066403 (2009).
- [40] T. Gould and J. F. Dobson, *J. Chem. Phys.* **138**, 014103 (2013).
- [41] E. Kraisler and L. Kronik, *Phys. Rev. Lett.* **110**, 126403 (2013).
- [42] A. Klein, *Phys. Rev.* **121**, 950 (1961).
- [43] R. van Leeuwen, N. Dahlen, G. Stefanucci, C.-O. Almbladh, and U. von Barth, *Introduction to the Keldysh Formalism and Applications to Time-Dependent Density Functional Theory* (Springer, Berlin, 2005).
- [44] G. Baym, *Phys. Rev.* **127**, 1391 (1962).
- [45] F. Caruso, D. R. Rohr, M. Hellgren, X. Ren, P. Rinke, A. Rubio, and M. Scheffler, *Phys. Rev. Lett.* **110**, 146403 (2013).
- [46] L. J. Sham and M. Schlüter, *Phys. Rev. Lett.* **51**, 1888 (1983).
- [47] M. Hellgren, D. R. Rohr, and E. K. U. Gross, *J. Chem. Phys.* **136**, 034106 (2012).
- [48] F. D. Sala and A. Görling, *J. Chem. Phys.* **115**, 5718 (2001).
- [49] J. C. Slater, *Phys. Rev.* **81**, 385 (1951).
- [50] M. Hellgren and U. von Barth, *Phys. Rev. B* **76**, 075107 (2007).
- [51] S. J. A. van Gisbergen, P. R. T. Schipper, O. V. Gritsenko, E. J. Baerends, J. G. Snijders, B. Champagne, and B. Kirtman, *Phys. Rev. Lett.* **83**, 694 (1999).
- [52] S. Kümmel, L. Kronik, and J. P. Perdew, *Phys. Rev. Lett.* **93**, 213002 (2004).
- [53] X. Gonze and M. Scheffler, *Phys. Rev. Lett.* **82**, 4416 (1999).
- [54] A. Görling and M. Levy, *Phys. Rev. B* **47**, 13105 (1993).